

A decade of earthquake activity at Taupō Volcano, New Zealand

 Finnigan Illsley-Kemp^{*α},  Pasan Herath^α,  Calum J. Chamberlain^α,  Konstantinos Michailos^β, and  Colin J. N. Wilson^α

^α School of Geography, Environment and Earth Sciences, Victoria University of Wellington, PO Box 600, Wellington, 6140, New Zealand.

^β Institute of Earth Sciences, University of Lausanne, Switzerland.

ABSTRACT

Taupō, New Zealand, is an active caldera volcano that in recent times has erupted on average every ~500 years, with the latest explosive eruption in 232±10 CE. Monitoring at Taupō is challenging as there has been no eruptive activity in documented history; however Taupō does undergo periods of unrest on roughly a decadal timescale, such as in 2019. Key to identifying these unrest periods is the establishment of what represents ‘normal’ inter-unrest activity. In this study, we generate and present a detailed earthquake catalogue for Taupō for 2010–2019 inclusive, consisting of 46,481 earthquakes. This record shows that the Taupō region has background earthquake rates of 50–200 earthquakes per month and that the 2019 unrest episode was preceded by an exponential increase in earthquake rate. We also show that when attenuation is accounted for there is no evidence for low-frequency earthquakes at Taupō, and that this is an important consideration for volcano monitoring as low-frequency earthquakes are often used to determine magma movement.

KEYWORDS: Seismology; Earthquake; Volcano-seismology; Taupo; Caldera; Monitoring.

1 INTRODUCTION

Monitoring of caldera volcanoes for potential signs of eruptive activity is challenging because of the infrequent yet potentially catastrophic nature of their eruptions [Wilson et al. 2021]. While all eruptions from caldera volcanoes are preceded by a period of unrest, only a small proportion of unrest periods lead to an eruption [Accolla et al. 2015]. Volcanic unrest is a broadly defined term but can generally be considered as a period of activity that is distinct from the background norm. Thus, in order to identify and define a period of unrest, one must also define what constitutes ‘normal’ activity. Here we consider the seismic record from Taupō volcano over a ten year period (2010–2019) of ‘normal’ activity against which to compare the unrest episode that occurred in 2019 [Illsley-Kemp et al. 2021].

Taupō is a large rhyolitic caldera volcano that lies within the Taupō Volcanic Zone (TVZ: Figure 1) in New Zealand’s North Island (Te Ika-a-Māui) [Barker et al. 2021]. The TVZ can be subdivided into three segments along its length. The southern and northern segments are characterised by andesite volcanism (e.g. Ruapehu and Whakaari/White Island), while the central segment is dominated by rhyolite volcanism and contains numerous caldera volcanoes that collectively make up the most productive region of Quaternary silicic volcanism on Earth [Wilson et al. 1995; 2009]. Volcanism in the TVZ is ultimately driven by the subduction of the Hikurangi plateau (Pacific plate) beneath the North Island (Australian plate) and the hyperactive volcanism at Taupō is fuelled by subcrustal basaltic magmas originating from high degrees of partial melting in the mantle wedge [Barker et al. 2020; Eberhart-Phillips et al. 2020]. The TVZ is also coincident with the Taupō continental rift, which has present day extension rates increasing from ≤5 mm yr⁻¹ at Ruapehu in the south to 13–19 mm yr⁻¹

at the Bay of Plenty in the north [Wallace et al. 2004; Lamarche et al. 2006; Villamor et al. 2017]. This manifests to the north of Taupō as the Taupō Fault Belt, which features several NE-trending normal faults with >100 m of surface displacement [Langridge et al. 2016].

Taupō volcano is largely concealed beneath Lake Taupō, which infills the caldera collapse structure and obscures most of the young vent sites [Barker et al. 2021, Figure 1]. The structural caldera is clearly defined by the largest negative gravity anomaly in the central North Island [Davy and Caldwell 1998; Stagpoole et al. 2021] and was primarily formed by the structural collapse associated with the 25.5 ka Oruanui supereruption [Wilson 2001]. The southern section of the lake does not coincide with a negative gravity anomaly but is also thought to have partially collapsed during the Oruanui eruption [Wilson 2001]. The southern margin of Taupō volcano coincides with the geological boundary that separates the rhyolitic central and andesitic southern TVZ, just northeast of Kākarama and Pi-hanga volcanoes (Figure 1). To the north, Taupo merges into the older domes of the Maroa volcanic centre. The 28 post-Oruanui eruptions (25 during the last 12 ka) range greatly in size and eruption style, with the latest and largest explosive event occurring at 232 ± 10 CE [Wilson 1993; Hogg et al. 2012; Barker et al. 2015; 2019; Hogg et al. 2019]. This 232 CE ‘Taupō eruption’ occurred in the northeast corner of the Oruanui caldera and caused further collapse [Davy and Caldwell 1998].

Seismic activity at Taupō is frequent. New Zealand’s seismic monitoring network (GeoNet, Petersen et al. [2011]) detects more than 300 earthquakes at Taupō every year. This ‘background’ activity has been punctuated by variably documented increases in earthquake activity on roughly a 10 year cycle [Eiby 1968; Gibowicz 1973; Hull and Grindley 1984; Grindley 1986; Sherburn 1992; Otway and Sherburn 1994; Johnston et al. 2002; Potter et al. 2015a; Barker et al. 2021],

*✉ finnigan.illsleykemp@vuw.ac.nz

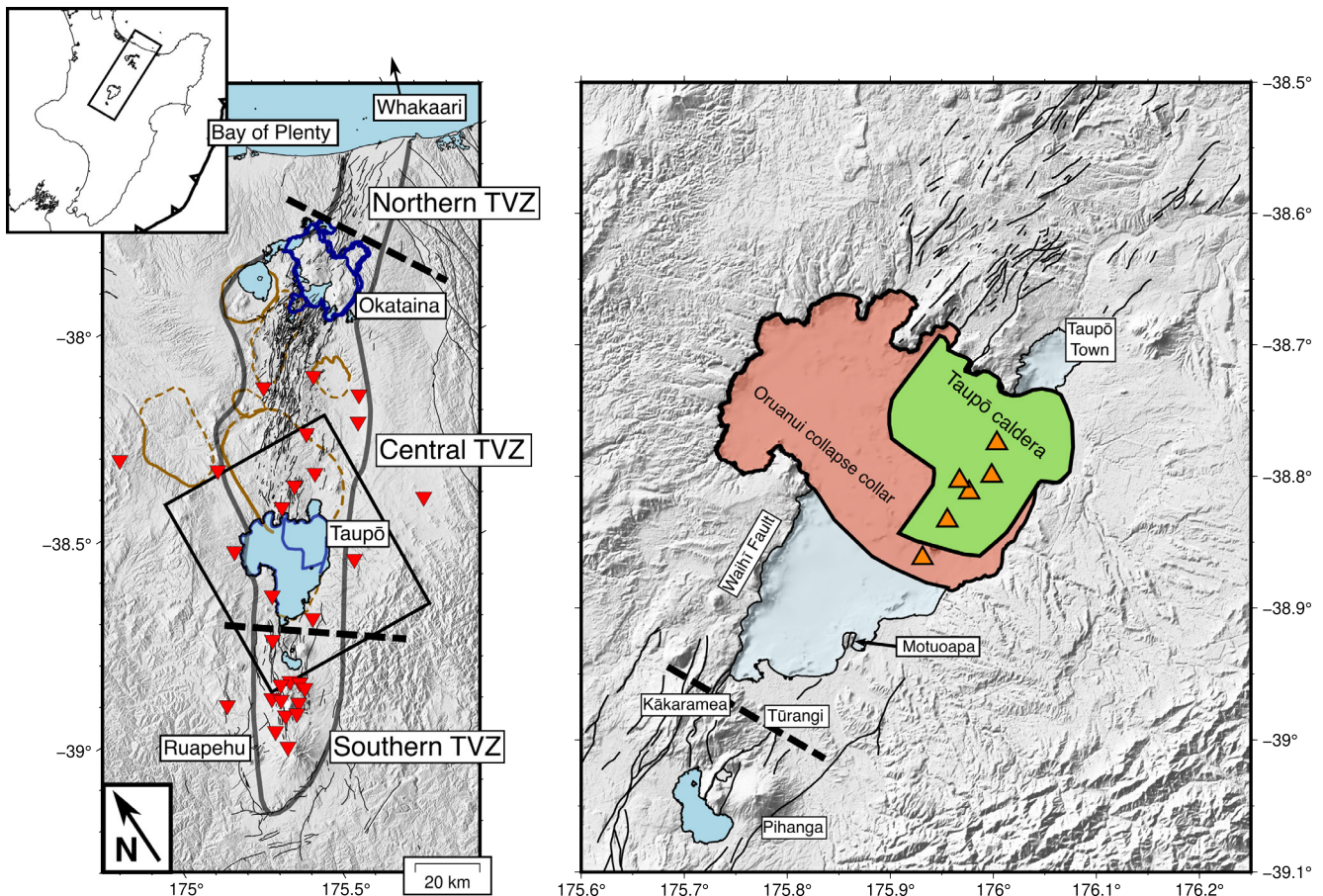


Figure 1: Left: The Taupō Volcanic Zone (TVZ) in New Zealand's North Island. The boundaries of the young TVZ (envelope around vents active in the last 350 kyr) is marked by the grey line, and is divided into the southern, central, and northern sections along its length. The central TVZ is dominated by caldera-related rhyolitic volcanism, whereas the southern and northern TVZ are characterised by andesite volcanism [Wilson et al. 1995; 2009]. Dark blue outlines denote the currently active calderas, Taupō in the south, and Okataina in the north, brown outlines denote older calderas. The mapped active faults are shown in black [Langridge et al. 2016]*. Red inverted triangles show the locations of the seismometers used in this study. Right: Major features of Taupō volcano. The red region denotes the Oruanui (25.5 ka) eruption collapse caldera and collar [Wilson 2001], the green region denotes the Taupō (232 CE) eruption collapse caldera [Davy and Caldwell 1998; Hogg et al. 2012]. The orange triangles denote vent locations from the last 2.15 ka of activity [Barker et al. 2015]. Figure adapted from Illsley-Kemp et al. [2021].

such as in 2019 [Illsley-Kemp et al. 2021]. The regular occurrence of seismicity makes monitoring of this volcano challenging as even periods of volcanic quiescence contain earthquake activity. Additional complexities arise because of the location of Taupō in an actively extending rift [$\sim 8 \text{ mm yr}^{-1}$; Villamor et al. 2017]. Making the distinction between 'normal' rift-related seismicity and any seismicity that can be attributed to volcanic processes is important in deciding what constitutes volcanic unrest. In this paper we produce a highly-detailed, 10 year earthquake catalogue for Taupō volcano and its surrounding region. We also search within this earthquake catalogue for low-frequency earthquakes, which have been attributed to volcanic unrest at many volcanoes worldwide [e.g. Hotovec-Ellis et al. 2018]. This catalogue is used to detail the behaviour of this volcano in its rifting setting in an inter-unrest time period.

2 DATA AND METHOD

2.1 Earthquake Detection and Location

We downloaded earthquake arrival time (pick) information from GeoNet [Petersen et al. 2011] for 2527 earthquakes that were detected, both by GeoNet and by manual inspection, in the Taupō region between 2010–2019 (inclusive). Each earthquake was manually inspected and picks were adjusted/added accordingly for the 29 regional GeoNet seismometers (9 broad-band, 20 short-period). These earthquakes were then located using NonLinLoc [Lomax et al. 2000] and a 1D velocity model based on a seismic-refraction study from the area [Stern and Benson 2011]. These earthquakes were then used to generate templates to find additional earthquake detections from continuous data using the matched-filter package EQcorrscan [Chamberlain et al. 2018].

For our matched-filter analysis we followed the same approach described in Illsley-Kemp et al. [2021]. Template wave-

* <http://data.gns.cri.nz/af/>

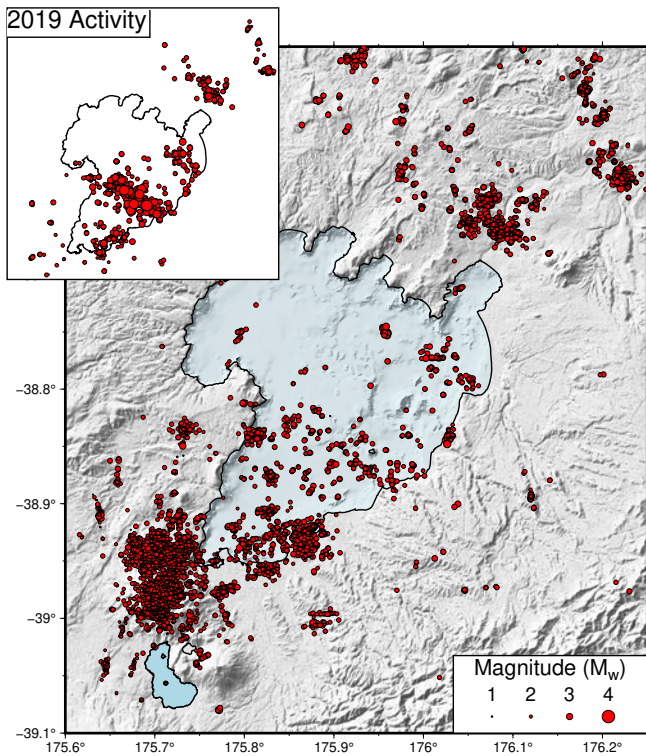


Figure 2: Main figure: The locations of all relocated earthquakes between 2010–2018 (inclusive). Inset: Relocated earthquakes during 2019 [Illsley-Kemp et al. 2021].

forms were filtered between 2–15 Hz and cut to 4 seconds length, starting 0.4 seconds before the P and S picks on the vertical and horizontal channels, respectively. Template waveforms were then correlated with continuous data between 2010-01-01 and 2019-12-31, which was also filtered between 2–15 Hz. Day-long normalised correlations were time-shifted to align with template moveouts and summed to generate day-long cross-correlation sums. Detections were made when the summed day-long correlations exceeded $0.4\times$ the number of channels. For each detection we then computed phase-picks derived from cross-correlations, following the approach outlined by Warren-Smith et al. [2017]. We only retained picks with normalised correlations of at-least 0.4, and events with picks on a minimum of four stations. This analysis resulted in a total of 46,481 earthquake detections between 2010–2019 (inclusive). We then located these earthquakes with NonLinLoc [Lomax et al. 2000] and the same 1D velocity model used to locate the template events. Each located earthquake was then assigned a unique ID number, based on the GeoNet format. If an earthquake in the catalog was also in the GeoNet catalogue, we used the GeoNet assigned ID (e.g. 2019p665658), if the event was detected and picked by the EQcorrscan procedure the ID has a ‘d’ flag (e.g. 2019d005968); finally, if the event was not recorded by GeoNet but was manually picked and used as a template it has an ‘m’ flag (e.g. 2019m000056). Direct comparisons between earthquakes that were located by our procedure and by GeoNet are difficult. As well as the velocity model and algorithm, the templates we used also have many more phase picks that were not included in routine

GeoNet locations; this particularly applied to S picks. Further, the vast majority of GeoNet locations at Taupō have ‘operator-assigned’ depths, and so depth comparisons are not possible.

We then generated differential pick times using waveform correlation on a 2 second window around each pick, 0.5 seconds before the pick, allowing the pick to adjust by up to 0.3 seconds. We computed differential pick-times for all event pairs within a maximum hypocentral separation of 8 km. These were then used to relocate the entire catalog using the double-difference relocation programme GrowClust [Trugman and Shearer 2017], requiring a minimum correlation of 0.6 and maximum cluster shifts of 2 km. Using this threshold we were able to relocate a total of 20,548 earthquakes, which we use for all subsequent analysis (Figure 2), with the exception of earthquake rates. The mean NonLinLoc-derived absolute 68 % confidence ellipsoid, representing absolute location errors for the subsequently relocated earthquakes, is ± 3.28 km and ± 3.76 km for the horizontal and vertical direction, respectively. The relative location errors derived from the internal GrowClust bootstrapping analysis for the relocated earthquakes are ± 0.85 km and ± 0.51 km for the horizontal and vertical directions, respectively.

2.2 Earthquake Magnitudes

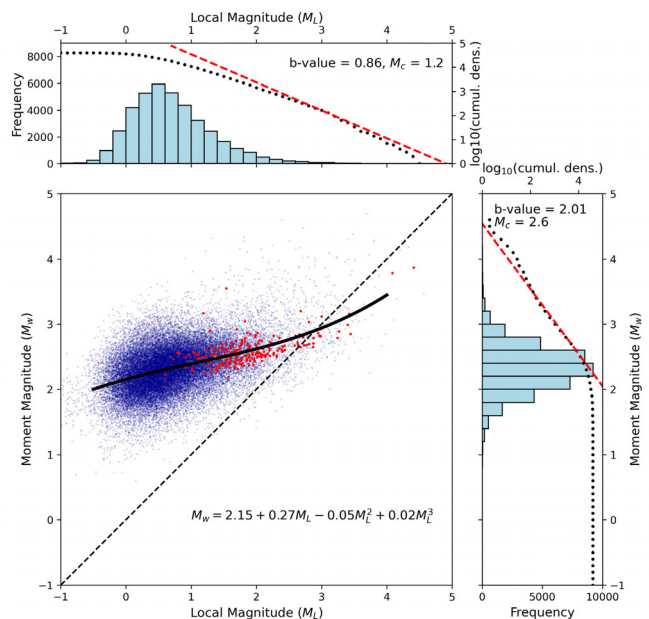


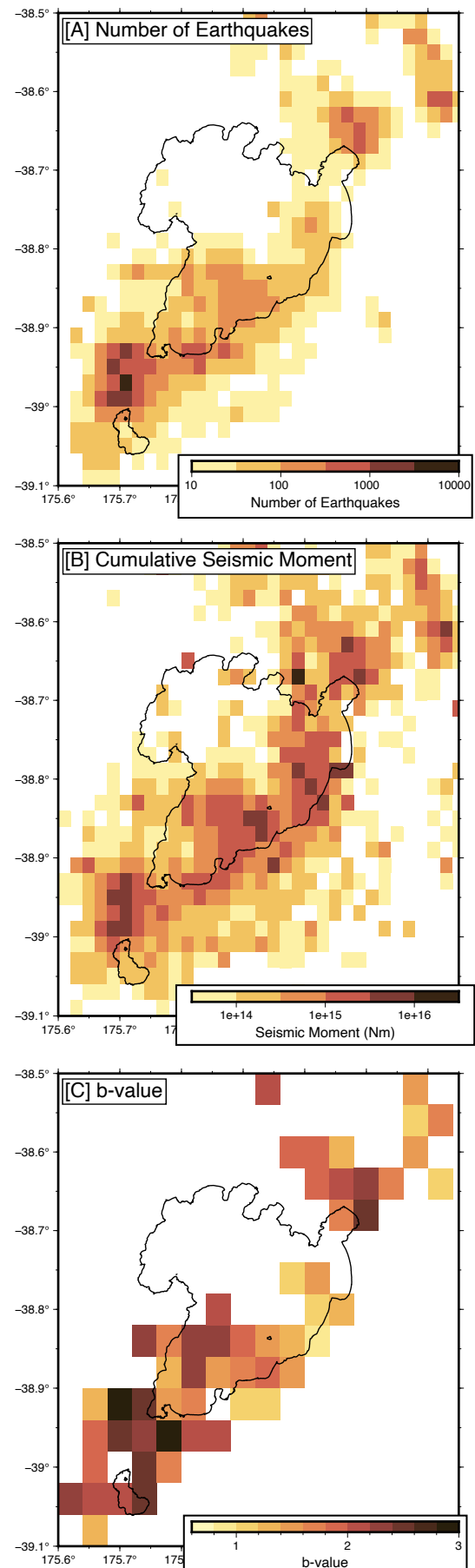
Figure 3: A comparison between local magnitude (M_L) and moment magnitude (M_W) values for the earthquake catalogue and respective b-values. The main panel shows that local magnitudes are lower than the equivalent moment magnitudes for $M_L < 2$. Red data points are earthquakes with a known radiation pattern. Each side panel shows the magnitude-frequency distribution and b-values for both local and moment magnitudes, b-values are calculated using the boundary-value-stability method [Roberts et al. 2015]. The b-values for local and moment magnitudes are 0.87 and 2.04 respectively, highlighting the discrepancy.

In order to calculate accurate local magnitudes (M_L) for the catalog we first convolved the seismograms (bandpass filtered between 1–20 Hz) for each earthquake with the Wood-Anderson standard response [Anderson and Wood 1925; Richter 1935] and measured the peak-to-peak displacement amplitude on the vertical component. We then use the local magnitude scale for Taupō from [Illsley-Kemp et al. 2021] to calculate local magnitudes while accounting for the local attenuation structure [Keir et al. 2006; Illsley-Kemp et al. 2017]. Recent work by Hudson et al. [2022] has shown that a local magnitude scale tends to underestimate magnitudes, particularly in volcanic regions with highly attenuating crust. Regions of high attenuation will cause the loss of high-frequency earthquake energy, which acts to reduce the maximum amplitude of a seismic phase in the time-domain. Deichmann [2017] has shown that this is likely to affect local magnitude measurements, but that this will not affect the measure of moment magnitude (M_W), as this is calculated using the long-period seismic energy. Therefore, in addition to local magnitudes we also calculate moment magnitudes using SeisSrcMoment [Hudson et al. 2022] (Table A1). This uses the spectral method of Stork et al. [2014] to measure the seismic moment (M_o) by fitting a Brune source model [Brune 1970] to the displacement spectrum of the seismic signal (Figure A1). The method uses the radiation pattern for P and S waves, which must be inverted for separately. Where available we use the radiation patterns inverted for in Illsley-Kemp et al. [2021] using MTFit [Pugh and White 2018]. For the vast majority of the earthquakes we assume an average radiation pattern [Hudson et al. 2022]. We then convert seismic moment into moment magnitude using the relationship of Hanks and Kanamori [1979]. Finally we calculate b-values both for the dataset as a whole (Figure 3) and for spatially discretised areas (Figure 4). For these calculations we use the boundary-value-stability method of Roberts et al. [2015] combined with the maximum likelihood method. For the spatially discretised dataset we limit our calculations to areas with at least 100 earthquakes, with many having far more than this, and calculate an individual magnitude of completeness for each area (Figure 4).

3 RESULTS

When we compare the results of moment magnitude (M_W) versus local magnitude (M_L) for the entire earthquake catalogue (Figure 3) we see a similar pattern to that reported by Hudson et al. [2022], namely that the local magnitude scale appears to underestimate earthquake magnitude for values less

Figure 4: [Right] [A] The cumulative spatial distribution of earthquakes. The region is divided into $0.02^\circ \times 0.02^\circ$ subregions and the number of earthquakes summed. [B] As above but earthquake magnitudes are converted into seismic moment release and summed. [C] Spatially discretised b-value calculations in $0.04^\circ \times 0.04^\circ$ subregions. Only regions with at least 100 earthquakes are used for the calculation and individual magnitudes of completeness are calculated.



than an M_L of 3. This relationship can be described by:

$$M_W = 2.15 + 0.27M_L - 0.05M_L^2 + 0.02M_L^3, \quad (1)$$

this relationship has a residual standard error of ± 0.31 . We see that earthquakes with a known radiation pattern (red dots in Figure 3) fit this relationship closely, whereas there is more scatter for earthquakes with an assumed radiation pattern. There are also 13 earthquakes in our catalogue which had moment magnitudes independently calculated by GeoNet, they are in good agreement within 0.5 magnitude units. The final earthquake catalogue has local magnitudes ranging from M_L -1.6 to 5.3 , with a magnitude of completeness (M_C) of 1.2 and a b-value of 0.86 (Figure 3). In contrast the moment magnitudes range from M_W 0.6 to 4.7 , with a magnitude of completeness of 2.6 and a b-value of 2.01 (Figure 3). Generally b-values are elevated (> 1) in all regions, but are particularly high in the Kākaramea, Waihi Fault, and Wairakei regions (Figures 1 and 4C).

The spatial distribution of the earthquakes is rather clustered (Figures 2 and 4). In particular there is a very active cluster of seismicity beneath Kākaramea volcano which shows clearly in both the distribution of earthquakes (Figure 4A) and cumulative seismic moment release (Figure 4B). Closer to Taupō caldera, earthquake activity is focused in three regions; in the south of the lake near Motuoapa, between Motutaiko Island and Karangahape Cliffs, and in the northeast of the caldera. The earthquakes in the 2019 volcanic unrest event reflected this distribution but with a far higher earthquake-rate [Illsley-Kemp et al. 2021]. To the northeast of the caldera, the earthquake activity clearly distinguishes the geothermal fields of Wairakei and Rotokawa [Sherburn et al. 2015; Hopp et al. 2019], though the former is less obvious in a map of cumulative seismic moment release (Figure 4). The region displays a relatively constant rate of earthquake activity, however there is a slight increase, in 2014, from fewer than 100 earthquakes a month to 100–200 earthquakes a month (Figure 5). This is punctuated by intense swarms beneath Kākaramea in 2015 and 2017. There is then a noticeable exponential increase in seismicity from mid-2018 up until the 2019 unrest event, before a rapid decrease [Illsley-Kemp et al. 2021].

The Kākaramea swarms will be described in detail separate to this manuscript. Here we describe the characteristics of the rest of the earthquake catalogue. The south of the lake, near the settlements of Tūrangi and Motuoapa, was one of the more seismically active parts of the region (Figure 6). Here, earthquakes tend to occur in rift-aligned (NNE–SSW) clusters between 7–10 km depth (b.s.l.). A large proportion of this seismic activity occurs beneath the Motuoapa peninsula, a complex of lava domes which last erupted ~ 35 ka [Kósik et al. 2021]. Further to the west, there is a cluster of seismicity near the Waihi fault scarp, between 8–9 km depth (Figure 7). The vast majority of these earthquakes ($> 90\%$) occurred in three spatially discrete clusters in 2016 and 2017 with no mainshock-aftershock pattern. With the exception of these three clusters, the Waihi fault region was seismically quiet over the 10 year study period. In the Taupō caldera region (Figure 8), the seismicity generally matches the distribution shown in the 2019 volcanic unrest [Illsley-Kemp et al. 2021], but in far smaller numbers.

Seismicity predominantly occurs between 6–12 km depth and there is very little earthquake activity in the region of the Horomatangi Reefs. To the northeast, there is highly clustered seismic activity near the four geothermal power plants and this occurs between 2–10 km depth (Figure 9). There is then an isolated earthquake cluster further to the north which appears to dip to the southwest at $\sim 40^\circ$.

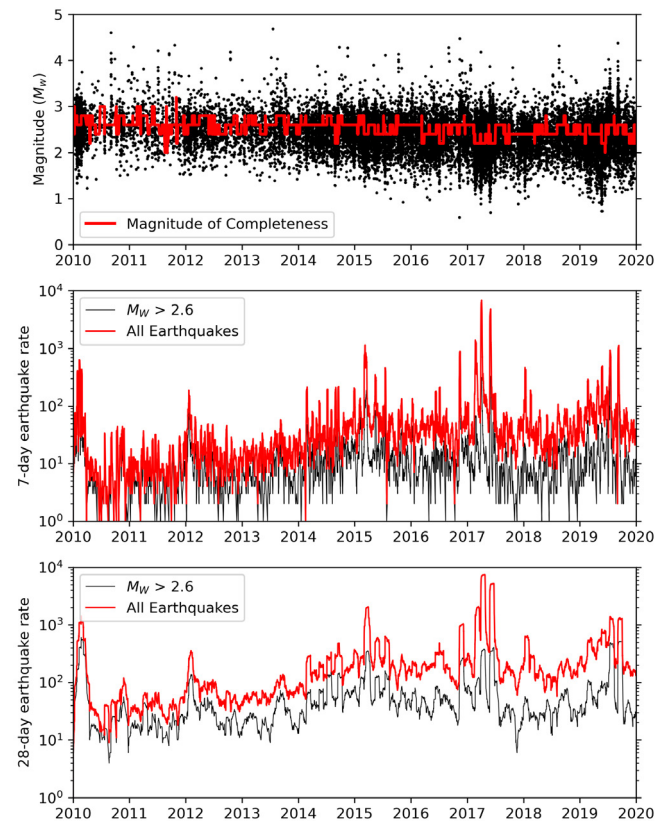


Figure 5: Rolling earthquake rates (i.e. cumulative number of earthquakes) for both 7- and 28-day time periods (backward-looking). Top shows the distribution of earthquake magnitudes through time and a rolling magnitude of completeness calculated over 28-day time-periods using the methodology of [Wiemer and Wyss 2000]. These calculations are made using the full earthquake catalogue of 46,481 earthquakes.

4 DISCUSSION

4.1 Earthquake activity at Taupō

Our 10-year study is the longest earthquake catalogue, aside from the GeoNet catalogue, that has been produced at Taupō and so provides insight into the earthquake activity on these time-lengths. Our results show that the ‘background’ rate of seismic activity at Taupō is relatively constant, however we do observe an increase in 2014 (Figure 5). Prior to this the 7- and 28-day earthquake rates were approximately 10 and 50, respectively. Then, following a $M_W 3$ earthquake near Motuoapa on 2014-02-21, the background 7- and 28-day earthquake rate for the region increases to approximately 50 and 200, respectively (Figure 5). By calculating the magnitude of completeness over a rolling time-window we can show that

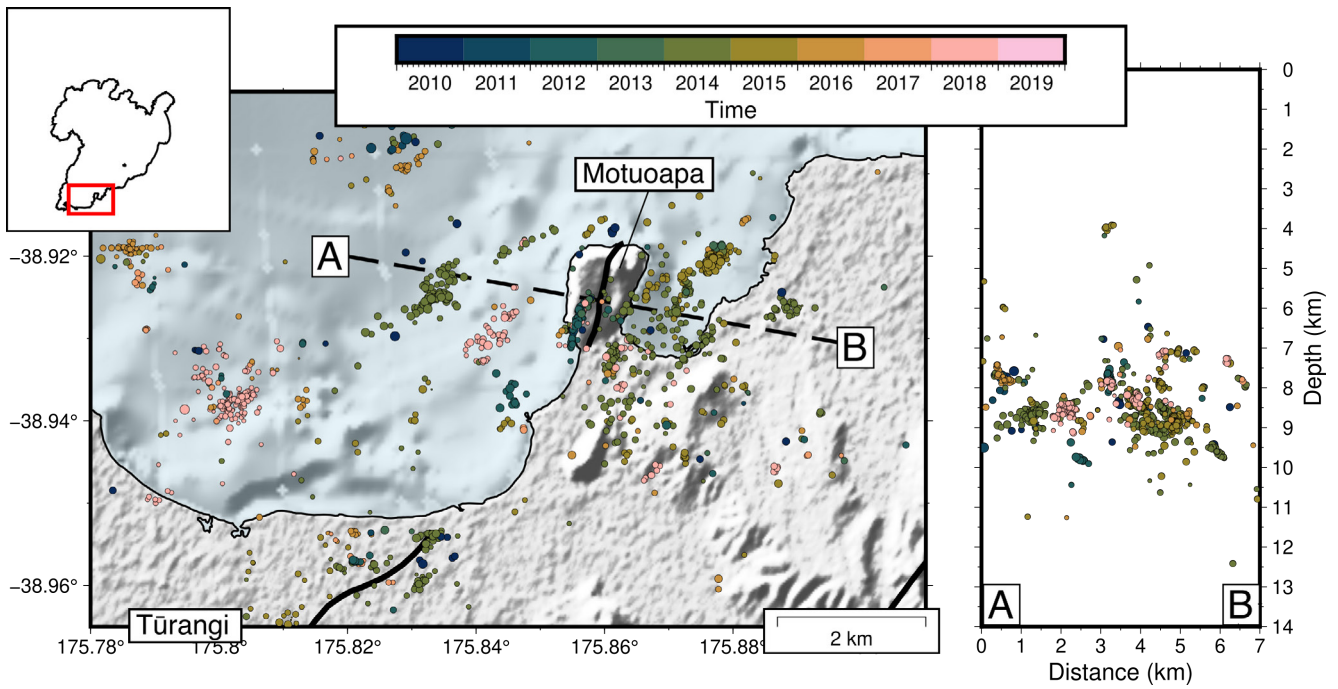


Figure 6: Earthquakes in the Tūrangi-Motuoapa region, coloured by origin time. The red box in the inset donates the location of the main panel. The cross-section is a 1:1 scale.

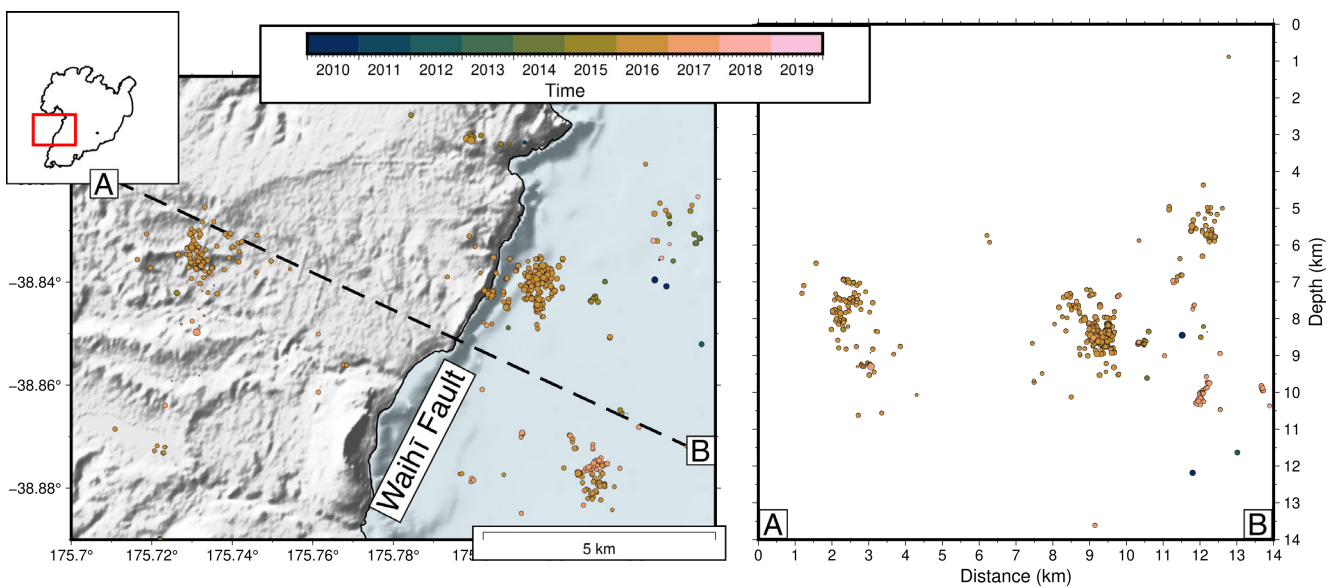


Figure 7: Earthquakes in the Waihi fault region, coloured by origin time. The red box in the inset donates the location of the main panel. The cross-section is a 1:1 scale.

this increase in earthquake rate was not due to an improvement in the earthquake detection, as the magnitude of completeness stays relatively constant at $M_W \sim 2.6$ for the whole ten-year time period. This background earthquake rate is punctuated by short periods of intense seismic activity, at some points in 2017 reaching rates of 10,000 earthquakes a week, though this was limited to swarms under Kākaramea and is unlikely to be directly related to Taupō volcano itself. There is also a noted increase in earthquake rate, in both the 7-day and 28-day average, from mid-2018 to September 2019.

This increase is exponential, resulting in an increase in 28-day earthquake rate from ~ 100 to ~ 1000 over a year. This increase in earthquake rate closely matches the onset of ground deformation at Taupō which culminated in the 2019 magmatic unrest [Illsley-Kemp et al. 2021]. The background earthquake rate shown here can be used as a useful indicator of what constitutes ‘normal’ activity at Taupō. This metric has been proposed as a key measure of unrest state for New Zealand volcanoes, and for Taupō specifically [Potter et al. 2015a; b]. In addition, earthquake rate is an important part of Bayesian

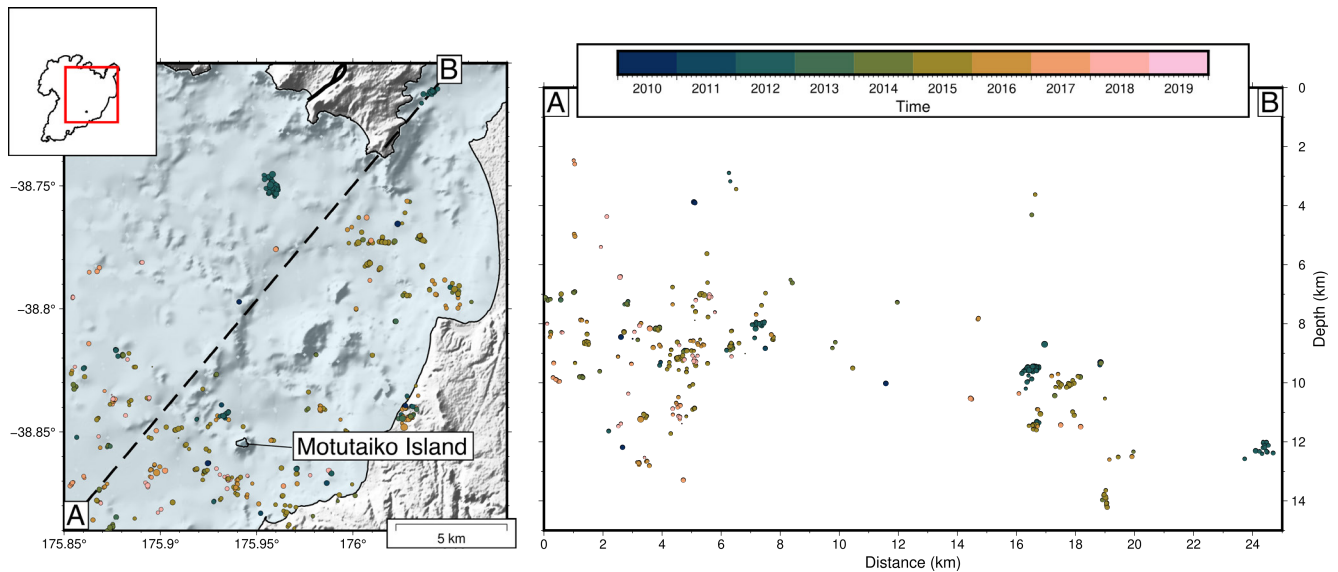


Figure 8: Earthquakes in the Taupō caldera region, coloured by origin time. The red box in the inset donates the location of the main panel. The cross-section is a 1:1 scale.

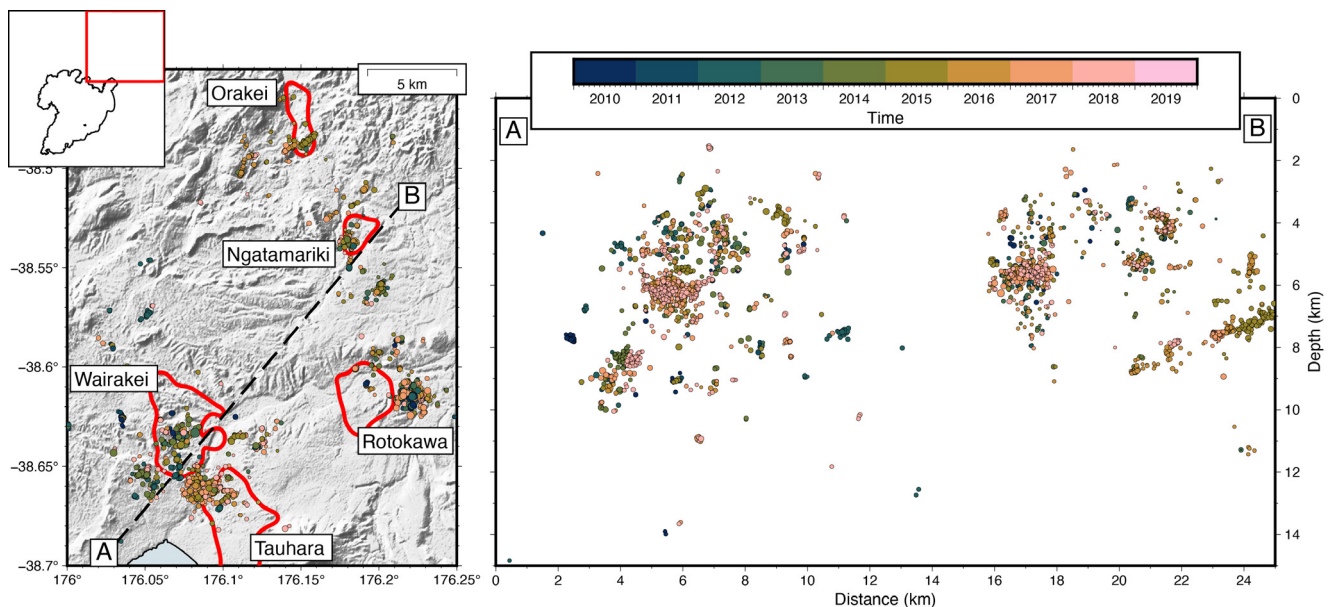


Figure 9: Earthquakes in the Wairakei-Rotokawa region, coloured by origin time. Red contours denote the 10 ohm resistivity contour taken from Bibby et al. [1995], which correlates low-resistivity zones to named geothermal fields. The red box in the inset donates the location of the main panel. The cross-section is a 1:1 scale.

Event Trees, which are increasingly being proposed as a monitoring and response tool at volcanoes worldwide [Constantinescu et al. 2016; Tierz et al. 2020].

In addition to earthquake rate, when considering whether earthquake activity is related to unrest at Taupō volcano one must of course consider the spatial location of the seismicity. Defining precise spatial boundaries for what defines Taupō volcano is not simple, as described by Barker et al. [2021], and has likely changed over time. We can suppose that earthquakes which occur in the region of the Taupō caldera, such as the 2019 unrest, are more likely to be directly associated with the modern magma reservoir [Illsley-Kemp et al. 2021].

In contrast the earthquake swarms in 2017, which caused rates of nearly 10,000 earthquakes per week (Figure 5), were situated beneath Kākaramēa outside of the area considered to be ‘Young Taupō’ [Barker et al. 2021], and thus may be unrelated to unrest within the Taupō magma reservoir. A similar argument follows with earthquake activity in the geothermal fields north of Taupō. Shallow seismicity here is likely to be influenced by geothermal power plant operations, however it is likely that these ‘satellite’ systems would be influenced by major unrest at Taupō and so heightened seismic activity here, particularly deep (>5 km) within the geothermal fields, should not be considered as entirely divorced.

Through calculating both local and moment magnitudes for our earthquake catalogue we have demonstrated the difference this can make to b-value calculation (Figure 3). If using local magnitudes, a b-value of 0.86 is calculated, whereas with moment magnitudes a b-value of 2.01 is produced. This is a large difference and would lead to differing interpretations about the seismic activity as b-values less than 1 are often associated with tectonic cycles, whereas values greater than 1 are linked to fluid-driven seismicity [Wyss 1973; Wyss et al. 2001; Wiemer and Wyss 2002]. Our findings therefore reiterate the results of Hudson et al. [2022] that moment magnitudes should be used when considering b-values in volcanic settings. b-values in our earthquake catalogue show relatively little spatial variation (Figure 4) and suggest that seismicity in the Taupō region is primarily driven by fluid-fault interactions, as similarly documented at Ngatamariki geothermal field [Hopp et al. 2019], and at other geothermal and volcanic regions [e.g. Greenfield et al. 2020].

Our earthquake results at Ngatamariki are in good agreement with the more detailed study of this system by Hopp et al. [2019] (Figure 9). They found that seismicity occurred in the northwest and southeast of the field, closely associated with the location of injection wells. Ngatamariki earthquakes presented in our study are 1–2 km deeper than those located by Hopp et al. [2019]; this is likely due to the Ngatamariki-specific velocity model used by Hopp et al. [2019]. Seismicity at Rotokawa geothermal field is confined to an area of approximately 2 km². This occurs between reinjection and production wells and has previously been attributed to cooling-driven contraction of the geothermal reservoir [Sherburn et al. 2015]. Finally, a cluster of seismicity occurs near the boundary of the Wairakei and Tauhara geothermal fields occurs (Figure 9). This cluster of seismicity is close to a reinjection site that began operating in 2011 [Sherburn et al. 2015]. Deep earthquakes (4–6 km) here have been interpreted as occurring on a fault structure [Sepulveda et al. 2013], however we see no evidence for this in our results. Seismicity rates at all these geothermal fields remains relatively constant during our study period. We note, however, that a particularly deep (8–9 km) cluster of seismicity to the south of the Wairakei field is composed of two distinct swarms in 2013 and 2019 (Figure 9).

It has often been suggested that volcanic earthquakes can be triggered by large, distal earthquakes [e.g. West et al. 2005; Yukutake et al. 2013; Aizawa et al. 2016] and this behaviour has been explicitly suggested for the TVZ in response to the 2016 Kaikōura earthquake [Peng et al. 2018; Yao et al. 2021]. We find no evidence that the Kaikōura earthquake triggered microseismicity in the Taupō region. However, we cannot discount that this event may have triggered very-low-frequency tremor which would likely be missed by our template-matching approach.

4.2 Frequency Analysis

Earthquake activity in volcanic regions has frequently been shown to include low-frequency (long-period) earthquakes which predominantly contain frequencies <5 Hz [e.g. Julian 1994; Chouet 1996; Neubeurg et al. 2000; Hotovec-Ellis et al. 2018]. These low-frequency earthquakes have been in-

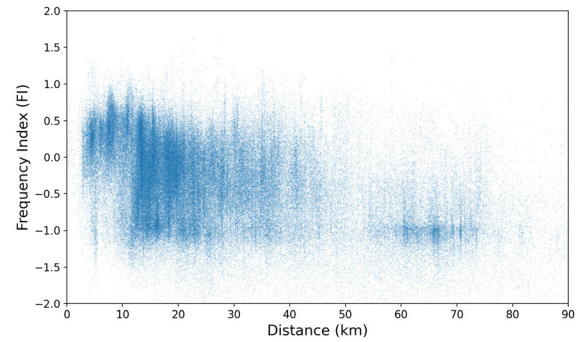


Figure 10: Hypocentral distance vs Frequency Index (FI) for 222,743 individual station-earthquake pairs recorded in this study.

terpreted to represent deformation involving aqueous fluids and/or magma. We therefore aimed to search the Taupō earthquake catalogue for examples of these low-frequency events. For each earthquake in our catalogue we calculate the Frequency Index (FI) [Buurman and West 2006]. The FI is a measure of the ratio between the high (7–11 Hz) and low (0.5–2 Hz) frequency energy content in each earthquake, which is then rescaled using a base 10 logarithm:

$$FI = \log_{10} \frac{A_H}{A_L}, \quad (2)$$

where A_H and A_L are the mean amplitudes in the high and low frequency bands respectively. By calculating a FI value for each earthquake-station pair (222,743 total measurements) we can see that FI decreases with distance (Figure 10). This trend is non-linear and in order to examine the FI of the earthquake at its origin we must remove the dependence of FI with distance. To achieve this we follow the approach of Greenfield et al. [2019]. By incorporating the effect of attenuation into Equation 2 we can see that:

$$FI(r) = \frac{r}{2Qv} (\overline{\omega_L} - \overline{\omega_H}) \log_{10} e + FIO, \quad (3)$$

where $FI(r)$ is the frequency index as a function of earthquake-station distance, r is distance, Q is the seismic quality factor, v is the seismic velocity, $\overline{\omega_L}$ and $\overline{\omega_H}$ are the mean angular frequencies in the lower and higher frequency bands, and FIO is the frequency index at the earthquake source. If we then consider the change of FI through a simple 1-D attenuation model we produce the equation:

$$FI(Q, r)_{i,k} = FIO_{i,k} + \log_{10} e \sum_j \frac{r_{i,j}}{Q_j v_j} (\overline{\omega_L} - \overline{\omega_H}) + C_k, \quad (4)$$

where FI for event i at station k includes the effect of attenuation (Q) through layer j , we also include the station correction term C_k . Equation 4 is in the form of $Ax = b$ and can be solved, using a least-squares approach, to give a value of FIO for every earthquake, stations corrections, and a 1-D

depth dependent Q model. We also include a regularisation matrix of the form,

$$\begin{bmatrix} 0 & & \dots & & & & 0 \\ & \ddots & & & & & \\ & & 0 & & & & \vdots \\ \vdots & & & -2 & 1 & & \\ & & & 1 & -2 & 1 & 0 \\ & & & & 1 & -2 & 1 \\ 0 & \dots & & 0 & 1 & -2 \end{bmatrix} \quad (5)$$

In order to calculate raypath lengths in individual depth layers we use the RAYINVR package [Zelt and Smith 1992] with the same 1D velocity model used for earthquake location. This produces the results shown in Figure 11. The 1D Q model shows that Q increases with depth through the crust and the obtained values broadly agree with the shallow results from the nationwide Q-inversion of Eberhart-Phillips et al. [2020]. We show that once attenuation is taken into account the FI values in-fact show no clear evidence for low-frequency earthquakes. On closer inspection, even earthquakes with the lowest corrected FI values (22 with FI less than -1) are in fact false detections generated by surface waves from large earthquakes ~ 2000 km to the north of New Zealand, in the Kermadecs.

While our analysis of earthquake frequency content could be considered a ‘null result’, it in fact has important implications for the monitoring of Taupō and volcanoes more generally. A key result of this modelling is that the uncorrected FI values (Figure 11A) could easily be interpreted as two populations of VT and LP earthquakes [e.g. Hotovec-Ellis et al. 2018]. However, once attenuation is accounted for the low-frequency population is removed and there is no evidence for low-frequency earthquakes. This agrees closely with experimental studies by Clarke et al. [2021] who used volcano parameters from Whakaari to show that intrinsic attenuation can make volcano-tectonic earthquakes resemble long-period seismicity. The implications for Taupō are that low-frequency earthquakes are either uncommon, or do not occur. Alternatively the GeoNet seismic network is too sparse to detect low-frequency earthquakes or low-frequency earthquakes were not sufficiently captured by our waveform templates and filtering. Therefore, low-frequency earthquakes should not necessarily be relied upon as a precursor to unrest/eruption at Taupō; for example, there was no evidence for low-frequency earthquakes before or during the demonstrably magmatic unrest event of 2019 [Hillsley-Kemp et al. 2021]. On the other hand, if genuine low-frequency earthquakes are observed at Taupō in the future they can be considered anomalous and of particular note for volcano monitoring. A densification of the seismic network at Taupō and routine consideration of attenuation may be necessary to identify future ‘true’ low-frequency earthquakes.

For volcano monitoring worldwide, we reiterate the findings of [Clarke et al. 2021] to suggest that great care must be taken when interpreting the frequency content of volcanic earthquakes. It is important to account for attenuation (both intrinsic and scattering) before asserting that low-frequency

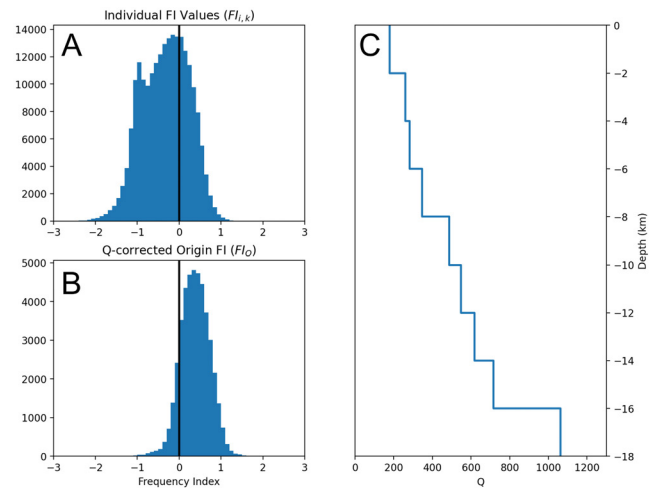


Figure 11: [A] Frequency index (FI) values for individual station-event pairs, before attenuation is accounted for. [B] The results of the inversion for attenuation-adjusted frequency index. [C] The resulting model of Q versus depth in 2 km depth slices.

earthquakes have occurred. This is particularly important for volcano monitoring networks which have relatively large distances between earthquake hypocentres and seismometers, like Taupō (Figure 10).

5 CONCLUSIONS

In this paper we present a detailed earthquake catalogue for the Taupō region, New Zealand, from 2010–2019. Our results show that:

- During the study period we detect and locate 46,481 earthquakes in the Taupō region. The majority of these occur outside of Taupō caldera and are likely driven by fluid-fault interactions.
- Background earthquake rates at Taupō are between 50–200 earthquakes per month. The 2019 unrest episode is preceded by an exponential increase in earthquake rate that coincides with the onset of ground deformation.
- b-values are elevated across the study region, with an overall b-value of 2.01, and we further confirm that it is important to use moment-magnitudes when calculating b-values in volcanic regions.
- Earthquake signals that are initially identified as low-frequency events are in fact volcano-tectonic earthquakes occurring within a highly attenuating region. There is no evidence for low-frequency earthquakes at Taupō, and attenuation must be accounted for in order to robustly identify such events.

AUTHOR CONTRIBUTIONS

FIK led the analysis and interpretation of the seismic data, and writing of the manuscript. PH, CJC, and KM assisted with the analysis of seismic data and contributed to writing of the manuscript. CJNW contributed to writing of the manuscript.

ACKNOWLEDGEMENTS

F. Illsley-Kemp and C.J.N. Wilson are supported by the ECLIPSE program, which is funded by the New Zealand Ministry of Business, Innovation and Employment (MBIE). F. Illsley-Kemp and C. J. Chamberlain are supported by the New Zealand Earthquake Commission Programme in Earthquake Seismology and Tectonic Geodesy at Victoria University of Wellington. We acknowledge the New Zealand GeoNet project and its sponsors EQC, GNS Science, LINZ, NEMA and MBIE for providing data used in this study. This project utilised the following open-source software, for which we thank the authors: Obspy [Beyreuther et al. 2010], PyRocko [Heimann et al. 2017], EQcorrscan [Chamberlain et al. 2018], SeisSrcMoment [Hudson et al. 2022], MTFit [Pugh and White 2018], Matplotlib [Hunter 2007], GMT [Wessel et al. 2019] and the Scientific Color Maps [Crameri 2021]. All digital elevation models use data from the Shuttle Radar Topography Mission (SRTM). The authors also wish to acknowledge the use of New Zealand eScience Infrastructure (NeSI) high performance computing facilities for this research. New Zealand's national facilities are provided by NeSI and funded jointly by NeSI's collaborator institutions and through the MBIE Research Infrastructure program. We also thank the thoughtful reviews of two anonymous reviewers.

DATA AVAILABILITY

All seismic waveform data is freely available from GeoNet (geonet.org.nz), and the final earthquake catalogue is freely available in QuakeML and text format at DOI: [10.5281/zenodo.6111982](https://doi.org/10.5281/zenodo.6111982).

COPYRIGHT NOTICE

© The Author(s) 2022. This article is distributed under the terms of the [Creative Commons Attribution 4.0 International License](https://creativecommons.org/licenses/by/4.0/), which permits unrestricted use, distribution, and reproduction in any medium, provided you give appropriate credit to the original author(s) and the source, provide a link to the Creative Commons license, and indicate if changes were made.

REFERENCES

- Acocella, V., R. Di Lorenzo, C. Newhall, and R. Scandone (2015). “An overview of recent (1988 to 2014) caldera unrest: Knowledge and perspectives”. *Reviews of Geophysics* 53(3), pages 896–955. DOI: [10.1002/2015RG000492](https://doi.org/10.1002/2015RG000492).
- Aizawa, K., H. Sumino, M. Uyeshima, Y. Yamaya, H. Hase, H. A. Takahashi, M. Takahashi, K. Kazahaya, M. Ohno, T. Rung-Arunwan, et al. (2016). “Gas pathways and remotely triggered earthquakes beneath Mount Fuji, Japan”. *Geology* 44(2), pages 127–130. DOI: [10.1130/G37313.1](https://doi.org/10.1130/G37313.1).
- Anderson, J. and H. O. Wood (1925). “Description and theory of the torsion seismometer”. *Bulletin of the Seismological Society of America* 15(1), pages 1–72. DOI: [10.1785/BSSA0150010001](https://doi.org/10.1785/BSSA0150010001).
- Barker, S. J., M. C. Rowe, C. J. N. Wilson, J. A. Gamble, S. M. Rooyakkers, R. J. Wysoczanski, F. Illsley-Kemp, and C. C. Kenworthy (2020). “What lies beneath? Reconstructing the primitive magmas fueling voluminous silicic volcanism using olivine-hosted melt inclusions”. *Geology* 48(5), pages 504–508. DOI: [10.1130/G47422.1](https://doi.org/10.1130/G47422.1).
- Barker, S. J., A. R. Van Eaton, L. G. Mastin, C. J. N. Wilson, M. A. Thompson, T. M. Wilson, C. Davis, and J. A. Renwick (2019). “Modeling ash dispersal from future eruptions of Taupo supervolcano”. *Geochemistry, Geophysics, Geosystems* 20(7), pages 3375–3401. DOI: [10.1029/2018GC008152](https://doi.org/10.1029/2018GC008152).
- Barker, S. J., C. J. N. Wilson, A. S. R. Allan, and C. I. Schipper (2015). “Fine-scale temporal recovery, reconstruction and evolution of a post-supereruption magmatic system”. *Contributions to Mineralogy and Petrology* 170(1). DOI: [10.1007/s00410-015-1155-2](https://doi.org/10.1007/s00410-015-1155-2).
- Barker, S. J., C. J. N. Wilson, F. Illsley-Kemp, G. S. Leonard, E. R. H. Mestel, K. Mauriohooho, and B. L. A. Charlier (2021). “Taupō: an overview of New Zealand's youngest supervolcano”. *New Zealand Journal of Geology and Geophysics* 64(2–3), pages 320–346. DOI: [10.1080/00288306.2020.1792515](https://doi.org/10.1080/00288306.2020.1792515).
- Beyreuther, M., R. Barsch, L. Krischer, T. Megies, Y. Behr, and J. Wassermann (2010). “ObsPy: A Python toolbox for seismology”. *Seismological Research Letters* 81(3), pages 530–533. DOI: [10.1785/gssrl.81.3.530](https://doi.org/10.1785/gssrl.81.3.530).
- Bibby, H. M., T. G. Caldwell, F. J. Davey, and T. H. Webb (1995). “Geophysical evidence on the structure of the Taupo Volcanic Zone and its hydrothermal circulation”. *Journal of Volcanology and Geothermal Research* 68(1-3), pages 29–58. DOI: [10.1016/0377-0273\(95\)00007-H](https://doi.org/10.1016/0377-0273(95)00007-H).
- Brune, J. N. (1970). “Tectonic stress and the spectra of seismic shear waves from earthquakes”. *Journal of Geophysical Research* 75(26), pages 4997–5009. DOI: [10.1029/JB075i026p04997](https://doi.org/10.1029/JB075i026p04997).
- Buurman, H. and M. E. West (2006). “Seismic precursors to volcanic explosions during the 2006 eruption of Augustine Volcano”. *The 2006 Eruption of Augustine Volcano, Alaska, U.S. Geological Survey Professional Paper*. Edited by J. A. Power, M. L. Coombs, and J. T. Freymueller. Volume 1769. US Geological Survey, pages 41–57. DOI: [10.3133/pp17692](https://doi.org/10.3133/pp17692).
- Chamberlain, C. J., C. J. Hopp, C. M. Boese, E. Warren-Smith, D. Chambers, S. X. Chu, K. Michailos, and J. Townend (2018). “EQcorrscan: Repeating and near-repeating earthquake detection and analysis in python”. *Seismological Research Letters* 89(1), pages 173–181. DOI: [10.1785/0220170151](https://doi.org/10.1785/0220170151).
- Chouet, B. A. (1996). “Long-period volcano seismicity: its source and use in eruption forecasting”. *Nature* 380(6572), pages 309–316. DOI: [10.1038/380309a0](https://doi.org/10.1038/380309a0).
- Clarke, J., L. Adam, and K. van Wijk (2021). “LP or VT signals? How intrinsic attenuation influences volcano seismic signatures constrained by Whakaari volcano parameters”. *Journal of Volcanology and Geothermal Research* 418 (107337). DOI: [10.1016/j.jvolgeores.2021.107337](https://doi.org/10.1016/j.jvolgeores.2021.107337).

- Constantinescu, R., R. Robertson, J. M. Lindsay, R. Tonini, L. Sandri, D. Rouwet, P. Smith, and R. Stewart (2016). “Application of the probabilistic model BET_UNREST during a volcanic unrest simulation exercise in Dominica, Lesser Antilles”. *Geochemistry, Geophysics, Geosystems* 17(11), pages 4438–4456. DOI: [10.1002/2016GC006485](https://doi.org/10.1002/2016GC006485).
- Crameri, F. (2021). “Scientific colour maps”. Version 7.0.0. *Zenodo Dataset*. DOI: [10.5281/zenodo.4491293](https://doi.org/10.5281/zenodo.4491293).
- Davy, B. W. and T. G. Caldwell (1998). “Gravity, magnetic and seismic surveys of the caldera complex, Lake Taupo, North Island, New Zealand”. *Journal of Volcanology and Geothermal Research* 81(1-2), pages 69–89. DOI: [10.1016/S0377-0273\(97\)00074-7](https://doi.org/10.1016/S0377-0273(97)00074-7).
- Deichmann, N. (2017). “Theoretical basis for the observed break in M_L/M_w scaling between small and large earthquakes”. *Bulletin of the Seismological Society of America* 107(2), pages 505–520. DOI: [10.1785/0120160318](https://doi.org/10.1785/0120160318).
- Eberhart-Phillips, D., S. Bannister, and M. Reyners (2020). “Attenuation in the mantle wedge beneath super-volcanoes of the Taupo Volcanic Zone, New Zealand”. *Geophysical Journal International* 220(1), pages 703–723. DOI: [10.1093/gji/ggz455](https://doi.org/10.1093/gji/ggz455).
- Eiby, G. (1968). “An annotated list of New Zealand earthquakes, 1460–1965”. *New Zealand Journal of Geology and Geophysics* 11(3), pages 630–647. DOI: [10.1080/00288306.1968.10420275](https://doi.org/10.1080/00288306.1968.10420275).
- Gibowicz, S. J. (1973). “Variation of frequency–magnitude relationship during Taupo earthquake swarm of 1964–65”. *New Zealand Journal of Geology and Geophysics* 16(1), pages 18–51. DOI: [10.1080/00288306.1973.10425384](https://doi.org/10.1080/00288306.1973.10425384).
- Greenfield, T., D. Keir, J.-M. Kendall, and A. Ayele (2019). “Seismicity of the Bora-Tullu Moye volcanic field, 2016–2017”. *Geochemistry, Geophysics, Geosystems* 20(2), pages 548–570. DOI: [10.1029/2018GC007648](https://doi.org/10.1029/2018GC007648).
- Greenfield, T., R. S. White, T. Winder, and T. Ágústsdóttir (2020). “Seismicity of the Askja and Bárðarbunga volcanic systems of Iceland, 2009–2015”. *Journal of Volcanology and Geothermal Research* 391 (106432). DOI: [10.1016/j.jvolgeores.2018.08.010](https://doi.org/10.1016/j.jvolgeores.2018.08.010).
- Grindley, G. W. (1986). “Historical Taupo earthquakes and earth deformation”. *Royal Society of New Zealand Bulletin* 24, pages 173–186.
- Hanks, T. C. and H. Kanamori (1979). “A moment magnitude scale”. *Journal of Geophysical Research* 84(B5), pages 2348–2350. DOI: [10.1029/JB084iB05p02348](https://doi.org/10.1029/JB084iB05p02348).
- Heimann, S., M. Kriegerowski, M. Isken, S. Cesca, S. Daout, F. Grigoli, C. Juretzek, T. Megies, N. Nooshiri, A. Steinberg, H. Sudhaus, H. Vasyura-Bathke, T. Willey, and T. Dahm (2017). “Pyrocko-An open-source seismology toolbox and library”. *GFZ Data Services*. DOI: [10.5880/GFZ.2.1.2017.001](https://doi.org/10.5880/GFZ.2.1.2017.001).
- Hogg, A. G., D. J. Lowe, J. Palmer, G. Boswijk, and C. B. Ramsey (2012). “Revised calendar date for the Taupo eruption derived by ^{14}C wiggle-matching using a New Zealand kauri ^{14}C calibration data set”. *The Holocene* 22(4), pages 439–449. DOI: [10.1177/0959683611425551](https://doi.org/10.1177/0959683611425551).
- Hogg, A. G., C. J. N. Wilson, D. J. Lowe, C. S. M. Turney, P. White, A. M. Lorrey, S. W. Manning, J. G. Palmer, S. Bury, J. Brown, J. Southon, and F. Petchey (2019). “Wiggle-match radiocarbon dating of the Taupo eruption”. *Nature Communications* 10(4669). DOI: [10.1038/s41467-019-12532-8](https://doi.org/10.1038/s41467-019-12532-8).
- Hopp, C., S. Sewell, S. Mroczek, M. Savage, and J. Townend (2019). “Seismic response to injection well stimulation in a high-temperature, high-permeability reservoir”. *Geochemistry, Geophysics, Geosystems* 20(6), pages 2848–2871. DOI: [10.1029/2019GC008243](https://doi.org/10.1029/2019GC008243).
- Hotovec-Ellis, A. J., D. R. Shelly, D. P. Hill, A. M. Pitt, P. B. Dawson, and B. A. Chouet (2018). “Deep fluid pathways beneath Mammoth Mountain, California, illuminated by migrating earthquake swarms”. *Science Advances* 4(8), eaat5258. DOI: [10.1126/sciadv.aat5258](https://doi.org/10.1126/sciadv.aat5258).
- Hudson, T. S., J.-M. Kendall, M. E. Pritchard, J. D. Blundy, and J. H. Gottsmann (2022). “From slab to surface: Earthquake evidence for fluid migration at Uturuncu volcano, Bolivia”. *Earth and Planetary Science Letters* 577 (117268). DOI: [10.1016/j.epsl.2021.117268](https://doi.org/10.1016/j.epsl.2021.117268).
- Hull, A. G. and G. W. Grindley (1984). “Active faulting near Taupo”. *EOS, Transactions of the American Geophysical Union* 65(7), pages 51–52. DOI: [10.1029/E0065i007p00051-03](https://doi.org/10.1029/E0065i007p00051-03).
- Hunter, J. D. (2007). “Matplotlib: A 2D graphics environment”. *Computing in Science & Engineering* 9(3), pages 90–95. DOI: [10.1109/MCSE.2007.55](https://doi.org/10.1109/MCSE.2007.55).
- Illsley-Kemp, F., S. J. Barker, C. J. N. Wilson, C. J. Chamberlain, S. Hreinsdóttir, S. Ellis, I. J. Hamling, M. K. Savage, E. R. Mestel, and F. B. Wadsworth (2021). “Volcanic unrest at Taupō volcano in 2019: Causes, mechanisms and implications”. *Geochemistry, Geophysics, Geosystems* 22, e2021GC009803. DOI: [10.1029/2021GC009803](https://doi.org/10.1029/2021GC009803).
- Illsley-Kemp, F., D. Keir, J. M. Bull, A. Ayele, J. O. Hammond, J.-M. Kendall, R. J. Gallacher, T. Gernon, and B. Goitorn (2017). “Local earthquake magnitude scale and b-value for the Danakil region of northern Afar”. *Bulletin of the Seismological Society of America* 107(2), pages 521–531. DOI: [10.1785/0120150253](https://doi.org/10.1785/0120150253).
- Johnston, D., B. Scott, B. Houghton, D. Paton, D. Dowrick, P. Villamor, and J. Savage (2002). “Social and economic consequences of historic caldera unrest at the Taupo volcano, New Zealand and the management of future episodes of unrest”. *Bulletin of the New Zealand Society for Earthquake Engineering* 35(4), pages 215–230. DOI: [10.5459/bnzsee.35.4.215-230](https://doi.org/10.5459/bnzsee.35.4.215-230).
- Julian, B. R. (1994). “Volcanic tremor: nonlinear excitation by fluid flow”. *Journal of Geophysical Research* 99(B6), pages 11859–11877. DOI: [10.1029/93JB03129](https://doi.org/10.1029/93JB03129).
- Keir, D., G. Stuart, A. Jackson, and A. Ayele (2006). “Local earthquake magnitude scale and seismicity rate for the Ethiopian Rift”. *Bulletin of the Seismological Society of America* 96(6), pages 2221–2230. DOI: [10.1785/0120060051](https://doi.org/10.1785/0120060051).

- Kósik, S., K. Németh, M. Danišik, J. N. Procter, A. K. Schmitt, B. Friedrichs, and R. B. Stewart (2021). “Shallow subaqueous to emergent intra-caldera silicic volcanism of the Motuoa Peninsula, Taupo Volcanic Zone, New Zealand—new constraints from geologic mapping, sedimentology and zircon geochronology”. *Journal of Volcanology and Geothermal Research* 411 (107180). DOI: [10.1016/j.jvolgeores.2021.107180](https://doi.org/10.1016/j.jvolgeores.2021.107180).
- Lamarche, G., P. M. Barnes, and J. M. Bull (2006). “Faulting and extension rate over the last 20,000 years in the offshore Whakatane Graben, New Zealand continental shelf”. *Tectonics* 25(4), TC4005. DOI: [10.1029/2005TC001886](https://doi.org/10.1029/2005TC001886).
- Langridge, R. M., W. F. Ries, N. J. Litchfield, P. Villamor, R. J. Van Dissen, D. J. A. Barrell, M. S. Rattenbury, D. W. Heron, S. Haubrock, D. B. Townsend, J. M. Lee, K. R. Berryman, A. Nicol, S. C. Cox, and M. W. Stirling (2016). “The New Zealand active faults database”. *New Zealand Journal of Geology and Geophysics* 59(1), pages 86–96. DOI: [10.1080/00288306.2015.1112818](https://doi.org/10.1080/00288306.2015.1112818).
- Lomax, A., J. Virieux, P. Volant, and C. Berge-Thierry (2000). “Probabilistic earthquake location in 3D and layered models”. *Modern Approaches in Geophysics* 18, pages 101–134. DOI: [10.1007/978-94-015-9536-0_5](https://doi.org/10.1007/978-94-015-9536-0_5).
- Neuberg, J., R. Luckett, B. Baptie, and K. Olsen (2000). “Models of tremor and low-frequency earthquake swarms on Montserrat”. *Journal of Volcanology and Geothermal Research* 101(1), pages 83–104. DOI: [10.1016/S0377-0273\(00\)00169-4](https://doi.org/10.1016/S0377-0273(00)00169-4).
- Otway, P. M. and S. Sherburn (1994). “Vertical deformation and shallow seismicity around Lake Taupo, New Zealand, 1985–90”. *New Zealand Journal of Geology and Geophysics* 37(2), pages 195–200. DOI: [10.1016/j.jvolgeores.2009.01.017](https://doi.org/10.1016/j.jvolgeores.2009.01.017).
- Peng, Z., B. Fry, K. Chao, D. Yao, X. Meng, and A. Jolly (2018). “Remote triggering of microearthquakes and tremor in New Zealand following the 2016 M W 7.8 Kaikōura earthquake”. *Bulletin of the Seismological Society of America* 108(3B), pages 1784–1793. DOI: [10.1785/0120170327](https://doi.org/10.1785/0120170327).
- Petersen, T., K. Gledhill, M. Chadwick, N. H. Gale, and J. Ristau (2011). “The New Zealand national seismograph network”. *Seismological Research Letters* 82(1), pages 9–20. DOI: [10.1785/gssrl.82.1.9](https://doi.org/10.1785/gssrl.82.1.9).
- Potter, S. H., B. J. Scott, G. E. Jolly, D. M. Johnston, and V. E. Neall (2015a). “A catalogue of caldera unrest at Taupo Volcanic Centre, New Zealand, using the Volcanic Unrest Index (VUI)”. *Bulletin of Volcanology* 77(78). DOI: [10.1007/s00445-015-0956-5](https://doi.org/10.1007/s00445-015-0956-5).
- Potter, S. H., B. J. Scott, G. E. Jolly, V. E. Neall, and D. M. Johnston (2015b). “Introducing the Volcanic Unrest Index (VUI): A tool to quantify and communicate the intensity of volcanic unrest”. *Bulletin of Volcanology* 77(77). DOI: [10.1007/s00445-015-0957-4](https://doi.org/10.1007/s00445-015-0957-4).
- Pugh, D. J. and R. S. White (2018). “MTfit: A Bayesian approach to seismic moment tensor inversion”. *Seismological Research Letters* 89(4), pages 1507–1513. DOI: [10.1785/0220170273](https://doi.org/10.1785/0220170273).
- Richter, C. (1935). “An instrumental earthquake magnitude scale”. *Bulletin of the Seismological Society of America* 25(1), pages 1–32. DOI: [10.1785/BSSA0250010001](https://doi.org/10.1785/BSSA0250010001).
- Roberts, N. S., A. F. Bell, and I. G. Main (2015). “Are volcanic seismic b-values high, and if so when?” *Journal of Volcanology and Geothermal Research* 308, pages 127–141. DOI: [10.1016/j.jvolgeores.2015.10.021](https://doi.org/10.1016/j.jvolgeores.2015.10.021).
- Sepulveda, F., J. Andrews, M. Alvarez, T. Montague, and W. Mannington (2013). “Overview of deep structure using microseismicity at Wairakei”. *35th New Zealand Geothermal Workshop: 2013 Proceedings*.
- Sherburn, S. (1992). “Seismicity of the Lake Taupo region, New Zealand, 1985–90”. *New Zealand Journal of Geology and Geophysics* 35(3), pages 331–335. DOI: [10.1080/00288306.1992.9514526](https://doi.org/10.1080/00288306.1992.9514526).
- Sherburn, S., C. Bromley, S. Bannister, S. Sewell, and S. Bourguignon (2015). “New Zealand geothermal induced seismicity: an overview”. *World Geothermal Congress, Melbourne, Australia*.
- Stagpoole, V., C. Miller, F. Caratori Tontini, T. Brakenrig, and N. Macdonald (2021). “A two million-year history of rifting and caldera volcanism imprinted in new gravity anomaly compilation of the Taupō Volcanic Zone, New Zealand”. *New Zealand Journal of Geology and Geophysics* 64(2-3), pages 358–371. DOI: [10.1080/00288306.2020.1848882](https://doi.org/10.1080/00288306.2020.1848882).
- Stern, T. and A. Benson (2011). “Wide-angle seismic imaging beneath an andesitic arc: Central North Island, New Zealand”. *Journal of Geophysical Research: Solid Earth* 116, B09308. DOI: [10.1029/2011JB008337](https://doi.org/10.1029/2011JB008337).
- Stork, A. L., J. P. Verdon, and J. M. Kendall (2014). “The robustness of seismic moment and magnitudes estimated using spectral analysis”. *Geophysical Prospecting* 62(4-Vertical Seismic Profiling and Microseismicity Frontiers), pages 862–878. DOI: [10.1111/1365-2478.12134](https://doi.org/10.1111/1365-2478.12134).
- Tierz, P., B. Clarke, E. S. Calder, F. Dessalegn, E. Lewi, G. Yirgu, K. Fontijn, J. M. Crummy, Y. Bekele, and S. Loughlin (2020). “Event trees and epistemic uncertainty in long-term volcanic hazard assessment of rift volcanoes: The example of Aluto (Central Ethiopia)”. *Geochemistry, Geophysics, Geosystems* 21(10), e2020GC009219. DOI: [10.1029/2020GC009219](https://doi.org/10.1029/2020GC009219).
- Trugman, D. T. and P. M. Shearer (2017). “GrowClust: A hierarchical clustering algorithm for relative earthquake relocation, with application to the Spanish Springs and Sheldon, Nevada, earthquake sequences”. *Seismological Research Letters* 88(2A), pages 379–391. DOI: [10.1785/0220160188](https://doi.org/10.1785/0220160188).
- Villamor, P., K. R. Berryman, S. M. Ellis, G. Schreurs, L. M. Wallace, G. S. Leonard, R. M. Langridge, and W. F. Ries (2017). “Rapid evolution of subduction-related continental intraarc rifts: The Taupo Rift, New Zealand”. *Tectonics* 36(10), pages 2250–2272. DOI: [10.1002/2017TC004715](https://doi.org/10.1002/2017TC004715).
- Wallace, L. M., J. Beavan, R. McCaffrey, and D. Darby (2004). “Subduction zone coupling and tectonic block rotations in the North Island, New Zealand”. *Journal of Geophysical Research: Solid Earth* 109(12), B12406. DOI: [10.1029/2004JB003241](https://doi.org/10.1029/2004JB003241).

- Warren-Smith, E., C. J. Chamberlain, S. Lamb, and J. Townsend (2017). “High-precision analysis of an aftershock sequence using matched-filter detection: The 4 May 2015 M_L 6 Wanaka earthquake, Southern Alps, New Zealand”. *Seismological Research Letters* 88(4), pages 1065–1077. DOI: [10.1785/0220170016](https://doi.org/10.1785/0220170016).
- Wessel, P., J. F. Luis, L. Uieda, R. Scharroo, F. Wobbe, W. H. F. Smith, and D. Tian (2019). “The generic mapping tools version 6”. *Geochemistry, Geophysics, Geosystems* 20(11), pages 5556–5564. DOI: [10.1029/2019GC008515](https://doi.org/10.1029/2019GC008515).
- West, M., J. J. Sánchez, and S. R. McNutt (2005). “Periodically triggered seismicity at Mount Wrangell, Alaska, after the Sumatra earthquake”. *Science* 308(5725), pages 1144–1146. DOI: [10.1126/science.1112462](https://doi.org/10.1126/science.1112462).
- Wiemer, S. and M. Wyss (2000). “Minimum magnitude of completeness in earthquake catalogs: Examples from Alaska, the western United States, and Japan”. *Bulletin of the Seismological Society of America* 90(4), pages 859–869. DOI: [10.1785/0119990114](https://doi.org/10.1785/0119990114).
- (2002). “Mapping spatial variability of the frequency-magnitude distribution of earthquakes”. *Advances in Geophysics* 45, pages 259–302. DOI: [10.1016/S0065-2687\(02\)80007-3](https://doi.org/10.1016/S0065-2687(02)80007-3).
- Wilson, C. J. N. (1993). “Stratigraphy, chronology, styles and dynamics of late Quaternary eruptions from Taupo volcano, New Zealand”. *Philosophical Transactions of the Royal Society A: Mathematical, Physical and Engineering Sciences* 343(1668), pages 205–306. DOI: [doi:10.1098/rsta.1993.0050](https://doi.org/10.1098/rsta.1993.0050).
- (2001). “The 26.5 ka Oruanui eruption, New Zealand: An introduction and overview”. *Journal of Volcanology and Geothermal Research* 112(1-4), pages 133–174. DOI: [10.1016/S0377-0273\(01\)00239-6](https://doi.org/10.1016/S0377-0273(01)00239-6).
- Wilson, C. J. N., G. F. Cooper, K. J. Chamberlain, S. J. Barker, M. L. Myers, F. Illsley-Kemp, and J. Farrell (2021). “No single model for supersized eruptions and their magma bodies”. *Nature Reviews Earth & Environment* 2(9), pages 610–627. DOI: [10.1038/s43017-021-00191-7](https://doi.org/10.1038/s43017-021-00191-7).
- Wilson, C. J. N., D. M. Gravley, G. S. Leonard, and J. V. Rowland (2009). “Volcanism in the central Taupo Volcanic Zone, New Zealand: Tempo, styles and controls”. *Studies in volcanology: the legacy of George Walker. Special Publications of IAVCEI* 2, pages 225–247. DOI: [10.1144/iaavel002.12](https://doi.org/10.1144/iaavel002.12).
- Wilson, C. J. N., B. F. Houghton, M. O. McWilliams, M. A. Lanphere, S. D. Weaver, and R. M. Briggs (1995). “Volcanic and structural evolution of Taupo Volcanic Zone, New Zealand: A review”. *Journal of Volcanology and Geothermal Research* 68(1-3), pages 1–28. DOI: [10.1016/0377-0273\(95\)00006-G](https://doi.org/10.1016/0377-0273(95)00006-G).
- Wyss, M., F. Klein, K. Nagamine, and S. Wiemer (2001). “Anomalously high b -values in the South Flank of Kilauea volcano, Hawaii: evidence for the distribution of magma below Kilauea’s East rift zone”. *Journal of Volcanology and Geothermal Research* 106(1), pages 23–37. DOI: [10.1016/S0377-0273\(00\)00263-8](https://doi.org/10.1016/S0377-0273(00)00263-8).
- Wyss, M. (1973). “Towards a physical understanding of the earthquake frequency distribution”. *Geophysical Journal of the Royal Astronomical Society* 31(4), pages 341–359. DOI: [10.1111/j.1365-246X.1973.tb06506.x](https://doi.org/10.1111/j.1365-246X.1973.tb06506.x).
- Yao, D., Z. Peng, Y. Kaneko, B. Fry, and X. Meng (2021). “Dynamic triggering of earthquakes in the North Island of New Zealand following the 2016 M_W 7.8 Kaikōura earthquake”. *Earth and Planetary Science Letters* 557(116723). DOI: [10.1016/j.epsl.2020.116723](https://doi.org/10.1016/j.epsl.2020.116723).
- Yukutake, Y., M. Miyazawa, R. Honda, M. Harada, H. Ito, M. Sakaue, K. Koketsu, and A. Yoshida (2013). “Remotely triggered seismic activity in Hakone volcano during and after the passage of surface waves from the 2011 $M_9.0$ Tohoku-Oki earthquake”. *Earth and Planetary Science Letters* 373, pages 205–216. DOI: [10.1016/j.epsl.2013.05.004](https://doi.org/10.1016/j.epsl.2013.05.004).
- Zelt, C. A. and R. B. Smith (1992). “Seismic traveltime inversion for 2-D crustal velocity structure”. *Geophysical Journal International* 108(1), pages 16–34. DOI: [10.1111/j.1365-246X.1992.tb00836.x](https://doi.org/10.1111/j.1365-246X.1992.tb00836.x).

APPENDIX A

The appendix contains further details of the moment magnitude calculations, including a comparison to GeoNet-derived magnitudes

Table A1: A comparison between moment magnitudes calculated by GeoNet and in this study.

GeoNet ID	GeoNet M_w	This study M_w
3247369	3.3	3.0
3254473	3.8	3.2
2015p495943	3.7	3.2
2016p634735	3.9	3.6
2017p235423	3.5	3.1
2017p237835	4.7	4.2
2017p445849	3.9	3.3
2019p472013	3.6	3.0
2019p524364	3.9	3.2
2019p665661	4.5	4.4
2019p665728	3.6	2.8
2019p809529	3.4	2.7
2019p840069	2.9	2.9

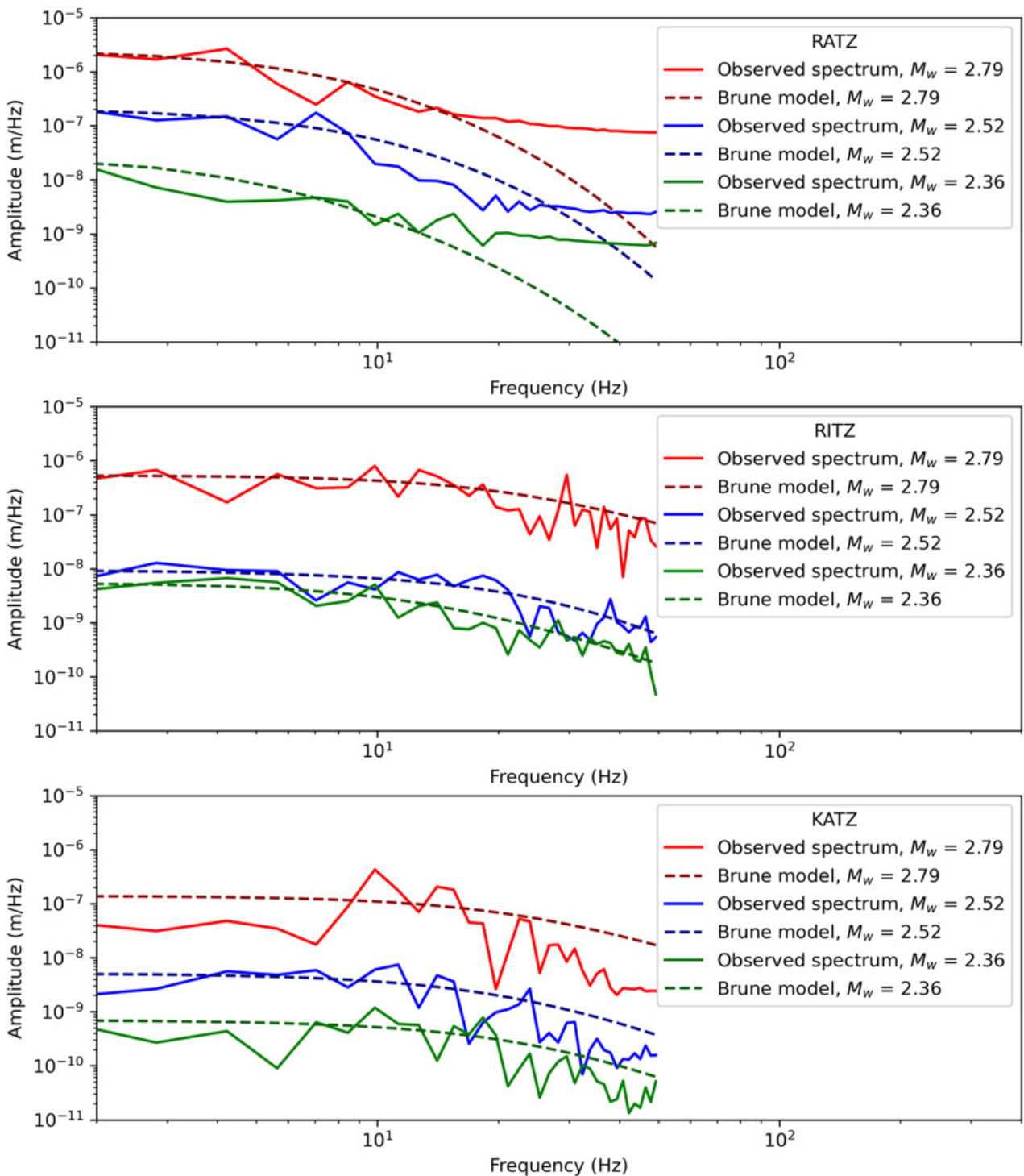


Figure A1: Examples of earthquake source displacement spectra (solid lines) for three separate earthquakes at stations RATZ, RITZ, and KATZ. Dashed lines show the best fitting Brune model.